Kondo Effect Mediated Topological Protection: Co on Sb(111)

Yinghui Yu,[†,‡] Limin She,[†,‡] Huixia Fu,[§] Min Huang,[†] Hui Li,[*,§] Sheng Meng,[§] and Gengyu Cao[*,†]

[†]State Key Laboratory of Magnetic Resonance and Atomic and Molecular Physics, Wuhan Institute of Physics and Mathematics, Chinese Academy of Sciences, Wuhan 430071, China and [§]Institute of Physics, Chinese Academy of Sciences, Beijing 100190, China. [‡]These authors contributed equally to this work.

ABSTRACT We report on a Kondo effect on Co/Sb(111) mediating topological protection of the surface states against local magnetic perturbations. A sharp scanning tunneling spectroscopic peak near the Fermi energy is interpreted as a fingerprint of the Kondo resonance with a high Kondo temperature of about 200 K. Density function theory calculations reveal that the protruding Co adatoms are responsible for the Kondo peak, while the Co atoms underneath present as nonmagnetic impurities. By identifying the quasiparticle interference wavevectors, we demonstrate that only scattering channels related to backscattering confinements are observed for surfaces with and without the Co adsorption. It suggests that the Kondo effect suppresses the backscattering of the topological surface states and may help to expand the functionality of magnetically coupled topological materials for spintronics applications.

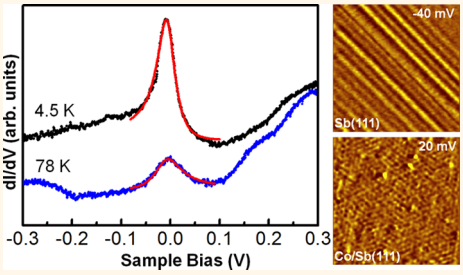

KEYWORDS: topological surface states · Sb(111) · Kondo effect · quasiparticle interference · time reversal symmetry

Novel topological surface states (TSS) of topological insulators (TIs) following a massless Dirac equation are protected by the time-reversal (TR) symmetry and insensitive to the spin-independent backscattering.[1,2] These remarkable properties ensure TIs as a promising material for applications in fields of spin electronic devices and quantum information processing.[3,4] Many experiments have already demonstrated that the chiral spin texture and TR symmetry forbid the electrons of TSS from backscattering by nonmagnetic defects.[5−9] Meanwhile, the TR symmetry of TSS may be locally broken by magnetic impurities,[10,11] which have attracted considerable interests in fields of condensed-matter physics. Up to now, numerous experimental works have focused on this aspect.[12−19] For example, Hasan's group found that Fe-deposited Bi_2Se_3 modified the topological spin structure systematically, leading to the TR symmetry breaking.[15] Nevertheless, later researches concluded that TSS of Bi_2Se_3 was tolerant to in-plane magnetic moments of Fe adatoms.[16,17] Moreover, cases of magnetic impurities such as manganese, iron, and gadolinium adsorbed on topological materials also indicated that the surface states could be remarkably insensitive to magnetic impurities that are not capable of breaking the TR symmetry.[18,19] Therefore, the stability of the TSS against local magnetic perturbations is still in controversy.

On the other hand, theoretical calculations predict that spin-polarized electronic clouds induced by the Kondo effect at the Fermi level (E_F) can screen the magnetic moments of local impurities and suppress the backscattering of the TSS.[20−25] Another recent experiment[26] on the Kondo insulator SmB_6 also implies the commonly observed Kondo interaction on noble metals[27−30] is compatible with the topological properties of the surface electrons which has been proved later.[31] Thus, one fundamental question to be addressed is whether the conventional Kondo effect generally exists on other topological surfaces doped by magnetic adsorbates and protects the TSS from magnetic scattering.

In this article, *via* scanning tunneling spectroscopy (STS) combined with the first-principles calculations, we investigate the local density of states (LDOS) of Co-atoms adsorbed Sb(111), of which the surface state is protected by the TR symmetry as studied by Angle-resolved photoemission spectroscopy (ARPES) and scanning tunneling microscopy (STM).[7,32,33] A sharp peak located near E_F is observed to

* Address correspondence to huili8@iphy.ac.cn, gycao@wipm.ac.cn.

Received for review August 27, 2014 and accepted October 28, 2014.

Published online October 28, 2014
10.1021/nn504817m

arise from the Kondo resonance. Furthermore, by carefully identifying the quasiparticle interference (QPI) patterns, we clarify that the scattering channels correspond only to the forbidden backscattering for surfaces with and without the Co adatoms. These results suggest that the TR symmetry of the Dirac Fermions is protected from the magnetic scattering by the Kondo resonance, which may expand the applications of magnetically coupled topological materials in spintronics.

RESULTS AND DISCUSSION

Figure 1a shows a typical STM topographic image recorded on clean Sb(111). The atomically resolved STM image (inset of Figure 1a) exhibits the hexagonal lattice structure where the lattice orientations are marked by arrows. Figure 1b shows a topographic image of Sb(111) with about 0.01 monolayer (ML) Co adsorption. The Co atoms form bright protrusions on the surface with typical lateral sizes ranging from 9 to 40 Å. Similar to the case of Co adsorption on the Pb films,[34] these protrusions can be identified as a single adsorbed atom or cluster, since Co atom and clusters can be simultaneously generated from the e-beam evaporator and some of the deposited Co atoms can combine into clusters by the surface diffusion as well. Interestingly, some Co atoms diffuse downward into the subsurface and exhibit an extended feature with a weak brightness as observed in Figure 1b. Here, the smallest bright protrusions were identified to be single Co atoms and other protrusions with larger sizes correspond to small Co clusters. In Figure 1c, line profile of a typical protrusion marked by a square (Figure 1b) reveals that the single Co atom with a circular shape possesses a height of ~1.0 Å and a size (full width at half-maximum) of ~9 Å, similar to the case of a single Co atom adsorbed on Cu(100) that shows a height of ~1.1 Å and a size of ~8 Å.[28]

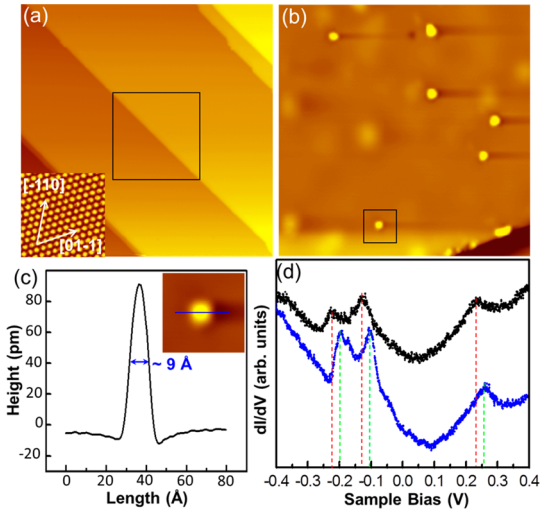

Figure 1. (a) A typical STM topography of Sb(111) (113 nm × 113 nm; U = 0.4 V; I = 30 pA). The inset shows an atomically resolved STM image where the lattice orientations are indicated by arrows. (b) A STM topography of Sb(111) with the 0.01-ML Co deposition (40 nm × 40 nm, U = 1.0 V, I = 20 pA). (c) Line profile taken along the line in the inset that is a zoomed-in STM image of the region indicated by a rectangle in (b). (d) dI/dV spectra recorded on Sb(111) with (blue) and without (black) the Co deposition. (set point: U = 0.4 V, I = 100pA).

To understand the LDOS evolution, STS measurements were performed on surfaces with and without the Co deposition (Figure 1d). The dI/dV curves exhibit very similar features of LDOS for both surfaces. There are three distinct peaks in the dI/dV spectra of clean Sb(111) located at the energies of −230, −120, and 230 meV, respectively. As previously reported,[32,33,35] the surface state bands of Sb(111) can be viewed as a distorted Dirac cone. The energy of the Dirac point is about −230 meV as revealed in Figure 1d. The peak features at about −120 and 230 mV correspond to the bending positions of the hole bands along the $\bar{\Gamma}-\bar{K}$ and $\bar{\Gamma}-\bar{M}$ directions, respectively.[33,35] The blue curve in Figure 1d shows the LDOS on Sb(111) with an ~0.01-ML Co coverage. Interestingly, we notice that the whole surface state of Sb(111) shifts *ca.* 25 meV toward the vacuum energy level after Co atoms are deposited. Similar band-shift characteristic has also been observed on other surfaces.[14,15,17−19] As larger electronegativity of antimony (Sb) is considered, it is naturally expected that a charge transfer from Sb to neighboring Co atoms would occur. Such charge redistribution should be responsible for a ~25 meV blue energy shift.

To investigate the quantum interaction between TSS and magnetic impurities, the dI/dV spectra were recorded at about 4.5 K by placing the STM tip at the center of a protruding Co atom (Figure 2a). The spectrum presents a sharp peak near E_F. Since the width of

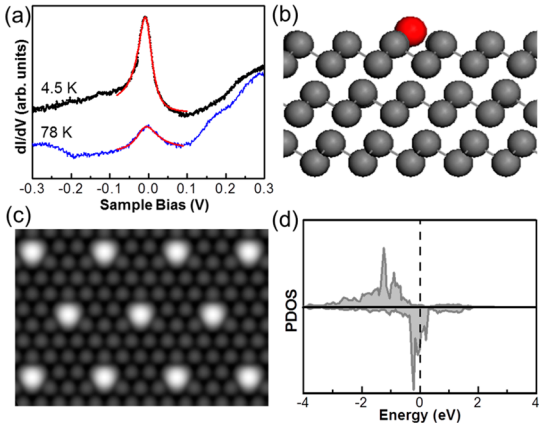

Figure 2. (a) dI/dV spectra recorded at the center of a protruding Co atom (set point: U = 0.4 V, I = 10 pA). The black and blue curves correspond to the measurement temperatures of about 4.5 and 78 K, respectively. The peaks are fitted by Fano function (red). (b) Geometric structure for Hollow-h configuration. Red and gray balls, respectively, denote Co and Sb atoms. (c) Simulated STM image for Hollow-h configuration. (d) Projected density of states (PDOS) on the Co atom for the Hollow-h configuration.

bare *d* band resonances are universal on the energy order of 100 meV[36,37] that is much larger than our observation and also the peak position are very close to E_F, the possibility of a *d* band resonance is excluded. This sharp peak feature is very similar to the previous observation of Co atom on noble metal surfaces, which is assigned as a fingerprint of Kondo resonance.[27−29] To confirm it, we further performed STS measurements at the temperature of about 78 K. As shown in the blue curve of Figure 2a, the peak around E_F still exists, but is strongly broadened. The thermal broadening feature is in accord with the characteristic of Kondo resonance and is mainly caused by the electron−electron scattering.[29] Therefore, here we believe that the sharp peak near E_F should be attributed to the Kondo effect resulted from the full screening of local magnetic impurities by surrounding spin-polarized electron clouds. Moreover, we also recorded the d*I*/d*V* spectra by placing the tips on top of the dipped Co atoms (Supporting Information Figure S1). No clues of Kondo resonance were observed at the vicinity of E_F, implying the nonmagnetic properties of these Co atoms.

To further reveal the origin of Kondo peak, first-principles calculations in the frame of density function theory (DFT) were performed on Co/Sb(111). Three stable adsorption configurations of Co atoms were found on both hollow and top sites of Sb(111) surface. The heights of Co atom with respect to the substrate surface, the adsorption energies and the local magnetic moments of the adsorption structures are listed in Table 1. The adsorption energies indicate the deposited Co atoms tend to dip into the Sb surface and locate at the hollow site, forming the most stable adsorption configuration named as Hollow-I (Supporting Information Figure S2a). The penetrated Co atom can also be stable on the top site of lower Sb atoms in the surface Sb(111) bilayer, named as Top-I (Supporting Information Figure S2b). However, in agreement to the STM observation, calculations also reveal the adsorbed Co atom can alternatively adopt a metastable configuration, in which the Co atom is above the topmost layer of Sb atoms and locates at the hollow site, named as Hollow-h (Figure 2b). The calculated height of Hollow-h Co is about 1.22 Å, very close to the STM measured height of the protruding Co atom in Figure 1c (about 1.0 Å). On the other hand, the simulated image obtained from the charge density between −1.0 eV and E_F (Figure 2c) is greatly consistent to the experimental images of above Co adatoms as shown in Figure 1b. These calculation results indicate that the Hollow-h configuration should correspond to the Co atoms above Sb surface. Meanwhile, the simulated STM images of Hollow-I (Supporting Information Figure S2c) and Top-I (Supporting Information Figure S2d) well correspond to the experimental STM image of underneath Co atoms in Figure 1b.

TABLE 1. Parameters of Metastable Adsorption Structures for Single Co Atom Deposited on Sb(111)[a]

str.	h_{Co} (Å)	E_a (eV)	M (μ_B)
Hollow-I	−1.48	4.28	0.00
Hollow-h	1.22	2.58	1.00
Top-I	0.14	3.59	0.00

[a] The h_{Co}, E_a, and M, are the height relative to the surface Sb layer, adsorption energy, and local magnetic moment per Co atom, respectively. Negative value of h_{Co} denotes that the Co atom is beneath the Sb surface.

On the basis of the calculations, the magnetic moment of isolated Co atom is reserved in the Hollow-h structure, while both the Hollow-I and Top-I structures are nonmagnetic. The projected density of states (PDOS) on Co atom of Hollow-h (Figure 2d) display asymmetrical peaks locating near E_F which are related to the large local magnetic moment of 1.0 μ_B (Bohr magneton) as revealed in Table 1. On the contrary, the PDOS plots for Hollow-I (Supporting Information Figure S2e) and Top-I (Supporting Information Figure S2f) structures show no net spin distributions near E_F, indicating the nonmagnetic feature. Therefore, the protruding Co adatoms, corresponding to the calculated Hollow-h configuraion, are responsible for the Kondo resonance observed in Figure 2a. The Kondo screening clouds and these Co adatoms combine into a many-body spin singlet state and serve as a nonmagnetic potential scatterer. Moreover, we also calculated the spin distribution for the Hollow-h Co adatom as revealed in Figures S2g,h of Supporting Information. It is found that its magnetic moment is highly localized around the Co position.

The observed line shape of Kondo resonance could be explained by the interaction between electrons and localized spins on the basis of the conventional Fano model,[38] as those in reported examples of magnetic impurities adsorbed on noble metals and on the topological Kondo insulator SmB_6.[26−30] The d*I*/d*V* spectra near E_F in Figure 2a can be fitted to a Fano function

$$\frac{dI}{dV} = A + B\frac{(\varepsilon+q)^2}{1+\varepsilon^2} \quad (1)$$

where A is the background d*I*/d*V* signal, B is the amplitude coefficient, $\varepsilon = (eV - \Delta E)/(\Gamma/2)$, q is the Fano line-shape factor, ΔE is the energy of the Kondo resonance, and Γ the full width of the resonance. The average fitting parameters ($\Delta E = -7.3 \pm 2$ meV, $q = -9.8 \pm 4.3$ meV, and $\Gamma = 50 \pm 6$ meV for about 4.5 K) are obtained through the d*I*/d*V* spectra recorded with different tips. Furthermore, the Kondo temperature T_k, another important signature, can be derived from Γ and T (temperature of measurement) based on the Fermi liquid theory[29] as

$$\Gamma = 2\sqrt{(\pi k_B T)^2 + 2(k_B T_K)^2} \quad (2)$$

where k_B is the Boltzmann constant. A high Kondo temperature, $T_k = 205 \pm 25$ K is acquired. Meanwhile,

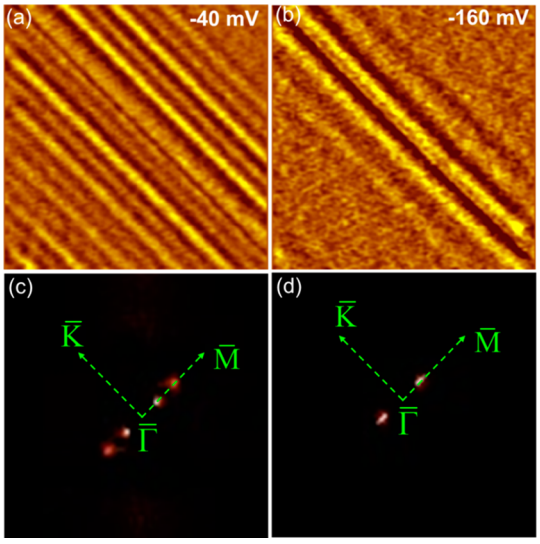

Figure 3. (a and b) Energy-resolved d*I*/d*V* maps of the region indicated by a rectangle in Figure 1a (51.5 nm × 51.5 nm, set point: *I* = 80 pA). (c and d) The corresponding FFT power spectra of (a and b). The reciprocal directions are marked by arrows.

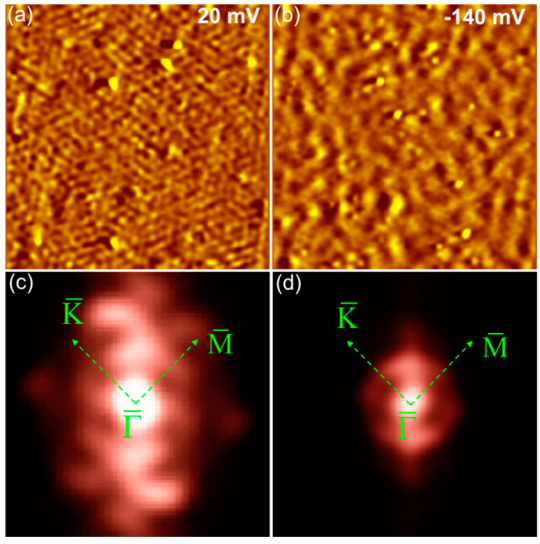

Figure 4. (a and b) Energy-resolved d*I*/d*V* maps recorded on ~0.01-ML Co deposited Sb(111) (100 nm × 100 nm, set point: *I* = 100 pA). (c and d) The corresponding FFT power spectra of (a and b). The reciprocal directions are marked by arrows.

we also fitted the d*I*/d*V* spectra recorded at about 78 K and the Kondo temperature is estimated to be 209 ± 40 K (Γ = 66 ± 8 meV), very close to the value obtained at ~4.5 K. In other words, the local spin of Co adatoms is fully confined by the Kondo screening electron cloud below the critical temperature.

The quantum interference fingerprints of TSS around Co impurities can be used for reflecting whether the Kondo interaction suppresses the backscattering of the TSS.[20−25] As shown in Figure 3a,b, energy-resolved d*I*/d*V* mappings at −40 and −160 meV on the clean Sb(111) surface (highlighted by a rectangle in Figure 1a) demonstrate that the line-shaped patterns along the straight step edge are similar to those commonly observed on noble metal surfaces.[39] Such patterns are ascribed to QPI of the electronic standing waves with different momenta. Two types of alternating patterns with different oscillation wavelengths are observed at −40 meV, leading to two different quantized wavevectors, $\mathbf{q}_1$ and $\mathbf{q}_2$, derived from fast Fourier transform (FFT) (see Figure 3c, in which the inner and outer spots correspond to $\mathbf{q}_1$ and $\mathbf{q}_2$, respectively.). However, only one type of oscillation patterns is observed at −160 meV, leading to one set of the wavevector displayed in the FFT image (Figure 3d). According to the previous study,[7] two types of oscillation patterns are identified as originating from the scattering between the adjacent hole pockets ($\mathbf{q}_1$) and from the interference between the centered electron and corner hole pockets with oppositely oriented momenta and parallel spins ($\mathbf{q}_2$). The observed wavevector in Figure 3d corresponds to $\mathbf{q}_2$, since $\mathbf{q}_1$ is vanished due to the overlap of the hole pockets into a hexagonal shape[34] at the energy below −120 meV. The Co adsorbed surface shows much richer interference fingerprint aroused from the surface state scattering around the Co defects, as shown in Figure 4a,b. Oscillation patterns with anisotropic shapes emerge at the vicinity of those adsorbed Co atoms. Two sets of extended bright spots reside around $\bar{\Gamma}$ as shown in Figure 4c. The regions with high intensities are all oriented along the $\bar{\Gamma} - \bar{M}$ directions, while the intensity along the $\bar{\Gamma} - \bar{K}$ directions vanishes. This feature should be ascribed to the hole bands of Sb(111) decaying into the bulk valence band in the $\bar{\Gamma} - \bar{K}$ direction at the energy of about −120 meV.[7,33,35] With the energy decreasing, the inner bright regions quickly shrink toward $\bar{\Gamma}$, but the outer ones are still visible at the $\bar{\Gamma} - \bar{M}$ direction, as seen from Figure 4 and Figure S3 of Supporting Information. At the energy of −140 meV (Figure 4d), the outer spots extend into a ring-like shape centering at $\bar{\Gamma}$.

Such scattering processes can be further understood by analyzing the possible origin of QPI wavevectors $\vec{q}$ in terms of the constant energy contour (CEC). In Figure 5a,b, we propose all possible scattering channels ($\mathbf{q}_1 - \mathbf{q}_4$) relating to QPI patterns along the $\bar{\Gamma} - \bar{M}$ direction. Since here all scattering processes occur at the $\bar{\Gamma} - \bar{M}$ direction, the interference vectors along the $\bar{\Gamma} - \bar{K}$ direction are not shown. The vectors $\mathbf{q}_1$ and $\mathbf{q}_2$ correspond to those on clean Sb(111) mentioned above, while the wavevector $\mathbf{q}_3$ ($\mathbf{q}_4$) corresponds to the QPI between electron (hole) pockets with oppositely oriented momenta and spin. As the topological protection nature is considered, $\mathbf{q}_3$ and $\mathbf{q}_4$ are related to the backscattering of Dirac Fermions. By measuring the interference patterns at various energy levels, the energy dispersions of the QPI phenomena along the $\bar{\Gamma} - \bar{M}$ direction were derived. To identify the

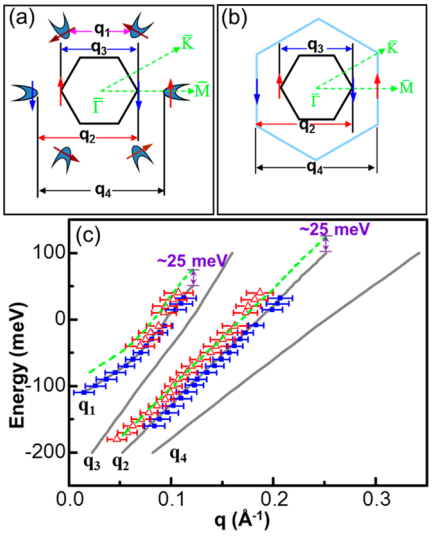

Figure 5. Schematic of CECs at the energies (a) above −120 meV and (b) below −120 meV. All of the possible interference wavevectors ($q_1 \sim q_4$) are shown along the $\bar{\Gamma} - \bar{M}$ directions. The arrows indicate the spin orientation of the Dirac Fermions. (c) Energy dispersions of the interference wavenumber. The triangular and rectangular points are obtained from the QPI patterns on the surfaces with and without Co adatoms, respectively. The solid curves correspond to the interference wavenumber ($q_1 - q_4$) calculated from previous STM and ARPES data. The dashed curves correspond to the shifted q_1 and q_2 with the energy shifting upward by 25 meV, respectively.

scattering channels, the previously published ARPES and STM data[7,32,33] are also used to calculate the interference vectors as a function of the quasiparticle energy. The dispersions of the four possible scattering processes are shown in Figure 5c as gray solid curves ($\mathbf{q}_1$ is obtained from previous STM data and $\mathbf{q}_2 \sim \mathbf{q}_4$ are calculated from ARPES data.). The triangular and rectangular points correspond to the QPI wavenumbers that are acquired from the Sb(111) surface with and without Co impurities, respectively. The positions of rectangular points greatly match the calculated $\mathbf{q}_1$ and $\mathbf{q}_2$ protected by the TR symmetry.[7] In addition, those values characterized by triangles wholly shift by *ca.* 25 meV toward the vacuum energy level in comparison with clean Sb(111). This dissimilarity is identical to the observation of d*I*/d*V* curves (Figure 1d), which is caused by the surface charge transfer. Considering the energy shift, accordingly, only the scattering channels protected by the TR symmetry are observed on the surfaces either with or without Co adatoms. That is to say, the backscattering of the TSS is still forbidden, although the large magnetic moments of protruding Co adatoms are employed.

A following straightforward question is whether the conventional Kondo effect observed on Co-doped Sb(111) surface influences the QPI between Dirac Fermions and magnetic impurities. According to recent theoretical studies,[22,24,25] Kondo screening electronic cloud is formed around magnetic adsorbates, which are fully screened for temperatures much below T_k. Similarly, T_k is much higher than the experimental temperature (~4.5 K), and the local magnetic moment of Co is also fully screened by the Kondo electron clouds, as revealed in the DFT calculations of spin distributions (Supporting Information Figures S2g,h). The Co adsorbates and the Kondo screening clouds combine into a many-body spin singlet state and serve as a nonmagnetic potential scatterer. Thus, the QPI fingerprints observed in Figure 4a,b originate from the TSS′ electrons scattering from the nonmagnetic Kondo state. On the other hand, as mentioned above, those dipped Co atoms observed in Figure 1b show no apparent magnetic moment and appear as nonmagnetic impurities. Thus, the TR symmetry of the TSS sustains on Co deposited Sb(111) as revealed in Figure 5c. In other words, Kondo screening protects the TSS from magnetic scattering.

CONCLUSIONS

In summary, a conventional Kondo effect with a high Kondo temperature is observed on protruding Co adatom by STS. Moreover, the QPI phenomena of the TSS around Co impurities are investigated by Fourier transform STM. No clues of broken TR symmetry are observed, although the surface state presents a blue energy shift of ~25 meV due to the surface charge transfer. It suggests that the Kondo screening might protect the TSS from magnetic scattering. These results provide a pathway to further understanding the interaction between the topological nontrivial states and magnetic adsorbates and may also be used to build novel spintronic devices in future.

METHODS

Experimental Details. Sb(111) substrate was cleaned *in situ* by repeated cycles of Ar^+ sputtering and subsequently annealing to about 620 K. Co atoms were deposited from an e-beam evaporator equipped with a high purity Co rod (2.0 mm diameter, 99.995% purity). The deposition rate was calibrated by measuring Co islands grown on Cu(111).[40] All measurements were carried out with an ultrahigh vacuum low temperature STM (Unisoku, Japan) at a base pressure better than 1×10^{-8} Pa. For better topography and energy resolution, all STM and STS measurements were performed at liquid helium temperature (about 4.5 K) with Pt−Ir tips. To evaluate the Kondo temperature, the STS measurements are also performed at the liquid nitrogen temperature (about 78 K). The d*I*/d*V* spectra were recorded by lock-in technique with a closed feedback loop. Sinusoidal modulation voltage with an amplitude of 4−6 mV at a frequency of about 1660 Hz was applied to the bias.

Computational Model. First-principles calculations in the frame of DFT were performed on Co/Sb(111) by using the Vienna Ab initio Simulation Package (VASP).[41] It is well-known that the dispersion interaction plays a significant role in both adsorption energy and geometry in such systems. Thus, the van der Waals density functional (vdw-DF), optB88-vdW,[42] was employed to better describe the interlayer interaction between Sb(111)

bilayers, as well as the Co−Sb interaction. The projector-augmented wave (PAW) pseudopotential was chosen to mimic the potentials of core electrons, combined with a plane wave basis set with the energy cutoff at 300 eV. The calculation model was constructed by three Sb(111) bilayers with a (4 × 4) periodicity, as well as a single deposited Co atom on the surface, and the vacuum region lager than 15 Å was applied. The Brillouin zone was sampled in (5 × 5 × 1) and (11 × 11 × 1) k-point meshes in structure relaxations and DOS calculations, respectively. All the structures were optimized until the force on each atom was less than 0.01 eV/Å.

Conflict of Interest: The authors declare no competing financial interest.

Supporting Information Available: The d*I*/d*V* spectra on dipped Co atoms; DFT calculations for Hollow-l and Top-l structures as well as calculated spin distribution for Hollow-h structure; d*I*/d*V* mapping and corresponding FFT images with two different bias voltages. This material is available free of charge *via* the Internet at http://pubs.acs.org.

REFERENCES AND NOTES

1. Hasan, M. Z.; Kane, C. L. Colloquium: Topological Insulator. *Rev. Mod. Phys.* **2010**, *82*, 3045.
2. Qi, X. L.; Zhang, S. C. Topological Insulators and Superconductor. *Rev. Mod. Phys.* **2011**, *83*, 1057–1110.
3. Burkov, A. A.; Hawthorn, D. G. Spin and Charge Transport on the Surface of a Topological Insulator. *Phys. Rev. Lett.* **2010**, *105*, 066802.
4. Leek, P. J.; Fink, J. M.; Blais, A.; Bianchetti, R.; Göppl, M.; Gambetta, J. M.; Schuster, D. I.; Frunzio, L.; Schoelkopf, R. J.; Wallraff, A. Observation of Berry's Phase in a Solid-State Qubit. *Science* **2007**, *318*, 1889–1892.
5. Hsieh, D.; Qian, D.; Wray, L.; Xia, Y.; Hor, Y. S.; Cava, R. J.; Hasan, M. Z. A Topological Dirac Insulator in a Quantum Spin Hall Phase. *Nature* **2008**, *452*, 970–975.
6. Roushan, P.; Seo, J.; Parker, C. V.; Hor, Y. S.; Hsieh, D.; Qian, D.; Richardella, A.; Hasan, M. Z.; Cava, R. J.; Yazdani, A. Topological Surface States Protected from Backscattering by Chiral Spin Texture. *Nature* **2009**, *460*, 1106–1110.
7. Seo, J.; Roushan, P.; Beidenkopf, H.; Hor, Y. S.; Cava, R. J.; Yazdani, A. Transmission of Topological Surface States through Surface Barriers. *Nature* **2010**, *466*, 343–346.
8. Zhang, T.; Cheng, P.; Chen, X.; Jia, J. F.; Ma, X. C.; He, K.; Wang, L. L.; Zhang, H. J.; Dai, X.; Fang, Z. Experimental Demonstration of Topological Surface States Protected by Time-Reversal Symmetry. *Phys. Rev. Lett.* **2009**, *103*, 266803.
9. Alpichshev, Z.; Analytis, J. G.; Chu, J. H.; Fisher, I. R.; Chen, Y. L.; Shen, Z. X.; Fang, A.; Kapitulnik, A. STM Imaging of Electronic Waves on the Surface of Bi_2Te_3: Topologically Protected Surface States and Hexagonal Warping Effects. *Phys. Rev. Lett.* **2010**, *104*, 016401.
10. Biswas, R. R.; Balatsky, A. V. Impurity-Induced States on the Surface of Three-Dimensional Topological Insulators. *Phys. Rev. B* **2010**, *81*, 233405.
11. Liu, Q.; Liu, C. X.; Xu, C.; Qi, X. L.; Zhang, S. C. Magnetic Impurities on the Surface of a Topological Insulator. *Phys. Rev. Lett.* **2009**, *102*, 156603.
12. Okada, Y.; Dhital, C.; Zhou, W.; Huemiller, E. D.; Lin, H.; Basak, S.; Bansil, A.; Huang, Y. B.; Ding, H.; Wang, Z. Direct Observation of Broken Time-Reversal Symmetry on the Surface of a Magnetically Doped Topological Insulator. *Phys. Rev. Lett.* **2011**, *106*, 206805.
13. Kou, X. F.; Lang, M. R.; Fan, Y. B.; Jiang, Y.; Nie, T. X.; Zhang, J. M.; Jiang, W. J.; Wang, Y.; Yao, Y. G.; He, L.; *et al.* Interplay between Different Magnetisms in Cr-Doped Topological Insulators. *ACS Nano* **2013**, *7*, 9205–9212.
14. Chen, Y. L.; Chu, J. H.; Analytis, J. G.; Liu, Z. K.; Igarashi, K.; Kuo, H. H.; Qi, X. L.; Mo, S. K.; Moore, R. G.; Lu, D. H.; *et al.* Massive Dirac Fermion on the Surface of a Magnetically Doped Topological Insulator. *Science* **2010**, *329*, 659–662.
15. Wray, L. A.; Xu, S. Y.; Xia, Y. Q.; Hsieh, D.; Fedorov, A. V.; Hor, Y. S.; Cava, R. J.; Bansil, A.; Lin, H.; Hasan, M. Z. A Topological Insulator Surface under Strong Coulomb, Magnetic and Disorder Perturbations. *Nat. Phys.* **2011**, *7*, 32–37.
16. Honolka, J.; Khajetoorians, A. A.; Sessi, V. T.; Wehling, O.; Stepanow, S.; Mi, J. L.; Iversen, B. B.; Schlenk, T.; Wiebe, J.; Brookes, N. B. In-Plane Magnetic Anisotropy of Fe Atoms on Bi_2Se_3(111). *Phys. Rev. Lett.* **2012**, *108*, 256811.
17. Scholz, M. R.; Sánchez-Barriga, J.; Marchenko, D.; Varykhalov, A.; Volykhov, A.; Yashina, L. V.; Rader, O. Tolerance of Topological Surface States towards Magnetic Moments: Fe on Bi_2Se_3. *Phys. Rev. Lett.* **2012**, *108*, 256810.
18. Noh, H. J.; Jeong, J.; Cho, E. J.; Lee, H. K.; Kim, H. D. Persistence of Surface States despite Impurities in the Surface of Topological Insulators. *Europhys. Lett.* **2011**, *96*, 47002.
19. Valla, T.; Pan, Z. H.; Gardner, D.; Lee, Y. S.; Chu, S. Photoemission Spectroscopy of Magnetic and Nonmagnetic Impurities on the Surface of the Bi_2Se_3 Topological Insulator. *Phys. Rev. Lett.* **2012**, *108*, 117601.
20. Tanaka, Y.; Furusaki, A.; Matveev, K. A. Conductance of a Helical Edge Liquid Coupled to a Magnetic Impurity. *Phys. Rev. Lett.* **2011**, *106*, 236402.
21. Feng, X. Y.; Chen, W. Q.; Gao, J. H.; Wang, Q. H.; Zhang, F. C. Anderson Impurity in a Helical Metal. *Phys. Rev. B* **2010**, *81*, 235411.
22. Žitko, R. Quantum Impurity on the Surface of a Topological Insulator. *Phys. Rev. B* **2010**, *81*, 241414(R).
23. Tran, M. T.; Kim, K. S. Probing Surface States of Topological Insulators: Kondo Effect and Friedel Oscillations in a Magnetic Field. *Phys. Rev. B* **2010**, *82*, 155142.
24. Mitchell, A. K.; Schuricht, D.; Vojta, M.; Fritz, L. Kondo Effect on the Surface of Three-Dimensional Topological Insulators: Signatures in Scanning Tunneling Spectroscopy. *Phys. Rev. B* **2013**, *87*, 075430.
25. Orignac, E.; Burdin, S. Kondo Screening by the Surface Modes of a Strong Topological Insulator. *Phys. Rev. B* **2013**, *88*, 035411.
26. Zhang, X. H.; Butch, N. P.; Syers, P.; Ziemak, S.; Greene, R. L.; Paglione, J. Hybridization, Inter-Ion Correlation, and Surface States in the Kondo Insulator SmB_6. *Phys. Rev. X* **2013**, *3*, 011011.
27. Madhavan, V.; Chen, W.; Jamneala, T.; Crommie, M. F.; Wingreen, N. S. Tunneling into a Single Magnetic Atom: Spectroscopic Evidence of the Kondo Resonance. *Science* **1998**, *280*, 567–569.
28. Knorr, N.; Schneider, M. A.; Diekhöner, L.; Wahl, P.; Kern, K. Kondo Effect of Single Co Adatoms on Cu Surfaces. *Phys. Rev. Lett.* **2002**, *88*, 096804.
29. Nagaoka, K.; Jamneala, T.; Grobis, M.; Crommie, M. F. Temperature Dependence of a Single Kondo Impurity. *Phys. Rev. Lett.* **2002**, *88*, 077205.
30. Kondo, J. Resistance Minimum in Dilute Magnetic Alloys. *Prog. Theor. Phys.* **1964**, *32*, 37–49.
31. Kim, D. J.; Xia, J.; Fisk, Z. Topological Surface State in the Kondo Insulator Samarium Hexaboride. *Nat. Mater.* **2014**, *13*, 466–470.
32. Hsieh, D.; Xia, Y.; Wray, L.; Qian, D.; Pal, A.; Dil, J. H.; Osterwalder, J.; Meier, F.; Bihlmayer, G.; Kane, C. L.; *et al.* Observation of Unconventional Quantum Spin Textures in Topological Insulators. *Science* **2009**, *323*, 919–922.
33. Gomes, K. K.; Ko, W.; Mar, W.; Chen, Y. L.; Shen, Z. X.; Manoharan, H. C. Quantum Imaging of Topologically Unpaired Spin-Polarized Dirac Fermions. 2009, arXiv:0909.0921v2. arXiv.org e-Print archive. http://arxiv.org/abs/0909.0921 (accessed Sep 4, 2009).
34. Zhang, X. Q.; Zhao, A. D.; Wang, K. D.; Xiao, X. D. Kondo Effect of Single Co Atoms Adsorbed on Pb/Si(111) Nanoislands. *Phys. Rev. B* **2008**, *78*, 035431.
35. Sugawara, K.; Sato, T.; Souma, S.; Takahashi, T.; Arai, M.; Sasaki, T. Fermi Surface and Anisotropic Spin-Orbit Coupling of Sb(111) Studied by Angle-Resolved Photoemission Spectroscopy. *Phys. Rev. Lett.* **2006**, *96*, 046411.
36. Weissmann, M.; Saúl, A.; Llois, A. M.; Guevara, J. Cobalt Impurities on Noble-Metal Surfaces. *Phys. Rev. B* **1999**, *59*, 8405–8407.
37. Vitali, L.; Ohmann, R.; Stepanow, S.; Gambardella, P.; Tao, K.; Huang, R. Z.; Stepanyuk, V. S.; Bruno, P.; Kern, K. Kondo

Effect in Single Atom Contacts: the Importance of the Atomic Geometry. *Phys. Rev. Lett.* **2008**, *101*, 216802.
38. Fano, U. Effects of Configuration Interaction on Intensities and Phase Shifts. *Phys. Rev.* **1961**, *124*, 1866–1878.
39. Crommie, M. F.; Lutz, C. P.; Eigler, D. M. Imaging Standing Waves in a Two-Dimensional Electron Gas. *Nature* **1993**, *363*, 524–527.
40. Vázquez de Parga, A. L.; García-Vidal, F. J.; Miranda, R. Detecting Electronic States at Stacking Faults in Magnetic Thin Films by Tunneling Spectroscopy. *Phys. Rev. Lett.* **2000**, *85*, 4365–4368.
41. Kresse, G.; Furthmüller, J. Efficient Iterative Schemes for *ab Initio* Total-Energy Calculations Using a Plane-Wave Basis Set. *Phys. Rev. B* **1996**, *54*, 11169–11186.
42. Klimeš, J.; Bowler, D. R.; Michaelides, A. van der Waals Density Functionals Applied to Solids. *Phys. Rev. B* **2011**, *83*, 195131.